

Dynamic Wettability on the Lubricant-Impregnated Surface: From Nucleation to Growth and Coalescence

Lin Guo, G. H. Tang,* and Satish Kumar*

Cite This: *ACS Appl. Mater. Interfaces* 2020, 12, 26555–26565

Read Online

ACCESS |



Metrics & More



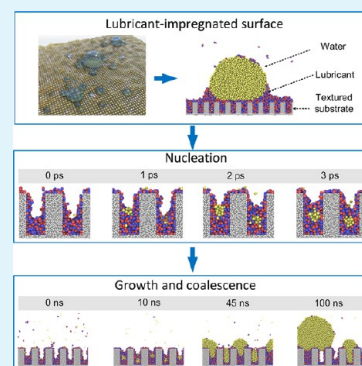
Article Recommendations



Supporting Information

ABSTRACT: The surface dynamic wettability during droplet nucleation and growth involved with phase change is different from the static wettability formed from a sessile drop. Revealing this dynamic wettability of the lubricant-impregnated surfaces (LISs) and identification of the consistency between the wettability during condensation and the static wettability are of significant importance. In this study, we investigated condensation of water droplets on LISs using molecular dynamics simulations. All possible morphologies on LISs were investigated considering the effects of interfacial tension and lubricant thickness. The exploration of droplet behaviors from nucleation to growth and coalescence revealed four nucleation mechanisms and six growth modes. The lubricant was observed to be beneficial for the formation of droplets and maintaining dropwise condensation mode. The present investigation also established that the consistency between the wettability during condensation and the static wettability was determined by the solid–water–oil interface and the lubricant thickness. A map was proposed which helps in deciding whether the wettability during condensation is the same as the static wettability on LIS.

KEYWORDS: lubricant impregnated surface, surface wettability, condensation, nucleation, droplet dynamic behaviors



INTRODUCTION

The wettability, that is, how liquids behave on a surface, is one of the fundamental properties of every solid and, thus, important for a wide range of natural systems as well as in many engineering applications.¹ From a theoretical point of view, Young's equation, formulated around 200 years ago, remains the fundamental equation in the science of wetting.² There are two commonly used methods to measure the contact angle: the sessile drop method³ and Wilhelmy plate method.⁴ The contact angle has been used to characterize the surface wettability and has been widely applied in both experimental and computational studies of interfacial science. Indeed, the contact angle has proved its suitability to characterize surface wettability in applications without phase change. However, when it comes to applications with phase change, like condensation, the characterization of contact angle might not work. For example, the surface with excellent superhydrophobicity can flood and lose function during condensation.⁵ Therefore, it is necessary to note here the two patterns of surface wettability: the static wettability and dynamic wettability during condensation (WDC). The sessile drop method or Wilhelmy plate method describes the surface static wettability, whereas the dynamic WDC refers to droplet states forming from nucleation, growth, and coalescence. In many cases, the WDC was considered as the same as the static wetting. However, the WDC behavior is not necessarily the same as the static wetting behavior. Mixing up these two

wettability patterns might cause improper applications of surfaces.

On the other hand, to overcome the limitation of traditional superhydrophobic and superoleophobic surfaces, Wong et al.⁶ proposed a bioinspired slippery liquid-infused porous surface combining the mechanical stability of a solid substrate with the liquid-like properties of the lubricant interface. Lafuma and Quéré⁷ pointed a hemiliquid and hemisolid materials where the liquid phase was trapped by the solid cavities. Smith et al.⁸ expanded the scope and brought all the different possible states together in a coherent framework under the lubricant impregnated surface (LIS) classification. The static wettability of LIS has been studied comprehensively by many researchers and applied in inkjet printing,⁹ droplet manipulation,^{10–15} anti-biofouling,^{16–19} water collection,²⁰ on-chip polymer synthesis,²¹ triboelectric nanogenerator,²² food safety,²³ optical devices,²⁴ blood contacting devices,²⁵ and so forth. Fundamental studies on LISs have also been conducted. Smith et al. described the thermodynamics of drops on lubricant-impregnated surfaces and showed that a drop on a lubricant-impregnated surface can exist in one of 12 different

Received: February 16, 2020

Accepted: May 18, 2020

Published: May 18, 2020



thermodynamic states depending on the properties of the working fluid droplet, impregnating lubricant, solid texture, and the surrounding environment.⁸ Guo et al. computationally studied and proposed eight possible droplet morphologies on LIS by considering the effects of lubricant thickness and surface geometry in addition to interfacial tension and substrate wettability.²⁶ LIS has also been successfully applied in applications with phase change, like condensation,^{27–30} anti-icing,^{31,32} anti-frosting,³³ and so forth. The nucleation details during condensation on LIS have also been experimentally investigated. Anand et al. found that the condensed droplets stayed afloat on the lubricant with minimal pinning to the surface by environmental scanning electron microscopy (ESEM) apparatus.³⁴ Xiao et al. fabricated an oil-infused surface by depositing (tridecafluoro-1,1,2,2-tetrahydrooctyl)-1-trichlorosilane on the surface with high-surface-energy sites on nanopillar tips. They found nucleation on pillar tips by ESEM, but pillar intervals and the oil–vapor interface were observed without nucleation.³⁵ Sun and Weisensee captured the side views of microdroplets self-propulsion during condensation on lubricant-infused surfaces.²⁹ Previous analyses were primarily based on the images recorded by video microscopy. However, video microscopy permits only the shape of the droplet–air interface to be monitored. The droplet–lubricant and the droplet–substrate interfaces remain hidden. To solve this problem, Kajiya et al. reported a 3D observation of condensing water on LIS using a laser scanning confocal microscope, imaging the drop surfaces as well as the drop–lubricant interface.³⁶ In addition to these experimental studies, a theoretical study on droplet nucleate sites and droplet growth behaviors was also conducted by Anand.³⁷ A framework was proposed to choose liquids that can lead to enhanced nucleation by examining the energy barriers.

However, knowledge about the WDC of LIS is yet incomplete. Several experimental studies have found that the droplet dynamics will be affected by the topology of the solid surface and the lubricant. However, the mechanism is yet unclear. Whether the static wettability characters remain the same in the dynamic wetting process is an important issue. Also, questions like whether the lubricant blocks the phase change process, where the water nucleates, and how the condensates grow and merge are to be answered. LIS is a complicated four-component system: water, vapor, lubricant, and substrate. Numerical methods have advantages in studying interfaces at nano/micro-scales compared to the experimental methods. Arenas et al. performed direct numerical simulations of liquid-infused surfaces and assessed its effect on the frictional, form and total drag for different textured geometries.³⁸ Metya and Singh studied the ice adhesion mechanism on lubricant-impregnated surfaces using molecular dynamics simulations.³⁹ Guo et al. investigated the droplet morphologies on LIS by the molecular dynamics method.²⁶ However, to the authors' best knowledge, simulations of the dynamic WDC on LIS are void.

The molecular dynamic method has been proved to be a powerful tool to capture interface states at nanoscale, and it has been successfully employed to study the condensation process on the superhydrophobic surface.^{40–42} In addition, the thermodynamic states of droplets on the lubricant-impregnated surface have been computationally studied.²⁶ The simulated results can predict all of the possible interface states and are consistent with the theoretical predictions in the study by Smith et al.,⁸ verifying the numerical method. Inspired by

these studies, we constructed a condensation process on the lubricant-impregnated surface (lubricant is also referred to oil, and denoted with subscript o). Droplet dynamic behaviors from nucleation to growth and coalescence on LIS are computationally studied, and comparisons between WDC and static wettability are also made. All of the 12 possible conditions on LIS can be summarized into four nucleation mechanisms and six growth modes. Finally, a map is developed to decide the consistency between the WDC and the static wettability. We believe that this work can shed light on fundamentally understanding the lubricant-impregnated surface and provide inspirations for LIS applications with a phase change.

METHOD

Simulation Setup and Procedures. Molecular dynamics simulation is performed using the LAMMPS package. To investigate the droplet WDC on LIS, the vapor–water–lubricant–solid system is built with dimensions of $345 \times 23.52 \times 1426.88 \text{ \AA}^3$ in the x , y , and z directions, respectively. The periodic boundary condition is applied in all directions. To build the lubricant-impregnated surface and save the computational time, hexane is chosen as the lubricant considering its relatively simple structure. Coarse-grained models are employed to represent water and hexane molecules, as shown in Figure 1a. A coarse-grained bead (W) represents four water molecules, and two coarse-grained beads represent one hexane molecule with each bead (CT) containing two CH_2 and one CH_3 groups. The solid pillars for exploring the condensation process are constructed using platinum (Pt) atoms. The width (w), height (h), and spacing (s) of these pillars are 15.68, 35.28, and 18.82 \AA , respectively. The Morse potential is employed for particle–particle interactions of water and hexane,⁴³ the 12/4 Lennard-Jones potential is employed for water and hexane interactions,⁴⁴ and the 12/6 Lennard-Jones potential is employed for interactions of Pt/water, Pt/hexane, and Pt/Pt.⁴⁰ Potential parameters for simulations in the present work are tabulated in Table 1. The energy parameters for constructing different interface states are explored and listed in the following section.

To study the WDC, a condensation system is built on LIS. The initial configuration of this four-component system is shown in Figure 1b. The liquid film at the top of the simulation box is used as a vapor source just like the macroscale condensation experiment, and the solid surface on top of the film is treated as the heat source (Pt_{up}). The solid surface on the bottom of the simulation box is treated as the surface for condensation (Pt_{down}) with lubricant on top of it. There are two steps of the simulation procedure. The hexane– Pt_{down} system and the water– Pt_{up} system are firstly separately equilibrated in an NVT ensemble at 300 and 550 K with a time step of 10 fs for 2 ns, shown as Step 1 in Figure 1b. Then, the water and hexane system is equilibrated in an NVE ensemble. Pt_{up} and Pt_{down} are equilibrated in an NVT ensemble at 550 and 300 K, respectively, shown as Step 2. Step 2 is running for 200 ns with a time step of 10 fs. Considering different time scales of nucleation and the droplet growing process, two types of snapshots are collected. The nucleation process is collected every 10 fs, an example of which is shown in Figure 1c. The droplets growing and coalescing process is collected every 1 ns, and Figure 1d is given as an example.

To study the static wettability, the hexane beads are first put on the solid surface with nanostructures and equilibrated at

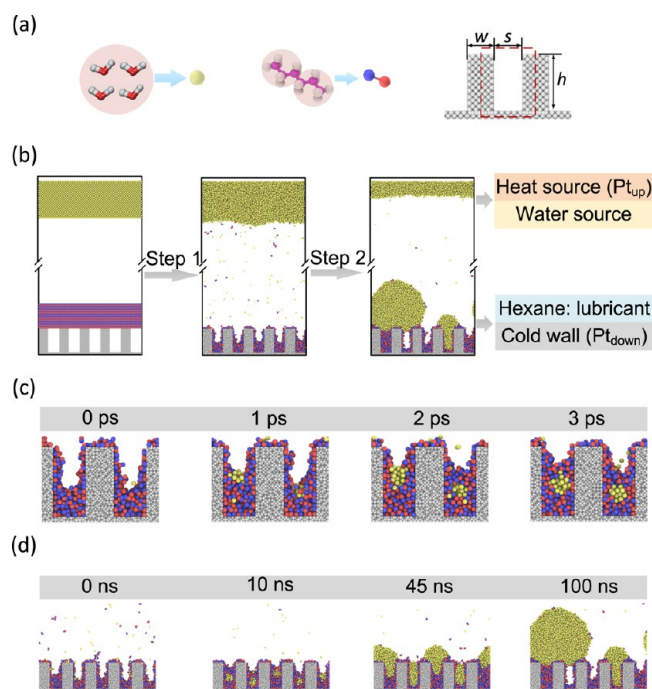


Figure 1. Schematic diagram of the simulation steps. (a) Coarse-grained bead represent four water molecules, and two beads represent a hexane molecule with each bead containing two CH₂ and one CH₃ groups. The nanostructure configuration w , s , and h refer to the width, spacing and height of nanopillars, respectively. (b) There are four parts of the condensation system: heat source (Pt_{up}) and water source on the top of the simulation box, and hexane (lubricant), and the cold wall (Pt_{down}) on the bottom of the simulation box. Two steps are conducted. Step 1: The hexane– Pt_{down} system and the water– Pt_{up} system are equilibrated separately in an NVT ensemble at 300 and 550 K, respectively; Step 2: The water and hexane system is equilibrated in an NVE ensemble and Pt_{up} and Pt_{down} are equilibrated in an NVT ensemble at 550 and 300 K, respectively. Two kinds of snapshots are collected according to different time scales: (c) nucleation process and (d) droplets growth and coalescence process.

Table 1. Potential Parameters

interaction site	potential	corresponding parameters			
		D_0 [kcal/mol]	α [\AA^{-1}]	r_0 [\AA]	r_c [\AA]
W–W	Morse	0.813	0.556	6.29	16
CT–CT	Morse	0.703	1.139	5.27	16
interaction site	potential	corresponding parameters			
		ϵ [kcal/mol]	σ [\AA]	r_c [\AA]	
Pt–Pt	12/6 LJ	16.07	2.471	13	
W–Pt	12/6 LJ		3.586	13	
CT–Pt	12/6 LJ		3.528	13	
interaction site	potential	corresponding parameters			
		ϵ [kcal/mole]	σ [\AA]	r_c [\AA]	
W–CT	12/4 LJ		4.642	15	

300 K using a Nose/Hoover thermostat with a time step of 10 fs for 0.5 ns. The computational box size is $510 \times 546 \times 994 \text{ \AA}^3$, and the periodic boundary condition is applied to all of the three directions. Then, 3130 water beads are used to generate a sessile droplet and added on the lubricant-impregnated surface. Finally, the system is equilibrated at 300 K using a Nose/Hoover thermostat with a time step of 10 fs for 0.5 ns, and snapshots of the droplet morphologies are collected.

Interfaces Explanations of LIS. The lubricant-impregnated surface is a complicated four-component system. To better comprehend the WDC on LIS, it is important to summarize interface states which can affect the WDC. There are three interfaces for a droplet on a roughed surface with the lubricant impregnated: interface A (water–air–oil), interface B (solid–water–oil), and interface C (solid–air–oil), as schematic in Figure 2a. In addition, from our experimental²⁸ and computational studies,²⁶ the lubricant thickness also affects droplet morphologies. Therefore, the lubricant thickness is considered here as an important factor in addition to the interface tension. All of the interface states are shown in Figure 2b. Specifically, there are two possible states for interface A: cloaking (the droplet is cloaked in the lubricant) and not cloaking (the droplet is not cloaked by the lubricant). Two states exist on interface B: encapsulated (the droplet keeps afloat on the lubricant and does not touch the substrate) and emerged (the droplet keeps afloat but touches the substrate). For interface C, the interface tension and lubricant thickness should be considered together. Thus, there are three states for interface C: encapsulated-rough (the substrate is fully wrapped by the lubricant and interface C is rough because of the thin lubricant), encapsulated-smooth (the substrate is wrapped by the lubricant and interface C is smooth due to the thick lubricant), and emerged (the lubricant is infused in pillar gaps but the substrate is exposed). The encapsulated-rough and emerged states are also marked as rough LIS, and the encapsulated-smooth is marked as smooth LIS. Therefore, there are 12 combinations in total of all of the possible interface states. For convenience of explanation of results, all of the 12 cases are listed and labeled, see Figure 2c. We mark the cases of smooth LIS as i+, ii+, v+, and vi+, representing thicker lubricant conditions of cases i, ii, v, and vi, respectively. To obtain the rough LIS and smooth LIS, two hexane numbers, 128 and 620, are applied in the static wettability simulation. As for the condensation simulation, to construct rough LIS and smooth LIS, the hexane numbers are 1120 and 2800, respectively. Energy parameters for constructing all of the cases are summarized in Table 2.

RESULTS AND DISCUSSION

Nucleation on LIS. Nucleation Sites. First, we investigate the nucleation behaviors for all of the 12 cases. For nucleation sites, there are three possible interfaces on LIS:³⁷ the air–solid interface (State I), the lubricant–solid interface (State II), and the air–lubricant interface (State III), as schematic in Figure 3a. The simulation results are listed in Tables 3 and 4. It shows that when interface B is in the emerged state, the nucleation occurs at the lubricant–solid interface (State II), including cases of ii, iii, vi, vii, ii+, and vi+. When interface B is in the encapsulated state, the nucleation occurs at the air–lubricant interface (State III), that is, cases i, iv, v, viii, i+, and v+.

To explore mechanisms underlying different nucleation sites, the associated free energies of nucleation for different states are examined. In State I, for nuclei forming on a solid surface in the presence of air environment, the total surface energy of the system is given by³⁷

$$E_1 = \gamma_{ws}A_{ws} + \gamma_{wa}A_{wa} - \gamma_{sa}A_{sa} = \psi_1 \pi \left(\frac{3V}{\pi \psi_1} \right)^{2/3} \gamma_{wa} \quad (1)$$

Here, γ is the interfacial tension, A is the surface area, and V is the droplet volume. The subscripts w , s , and a represent water,

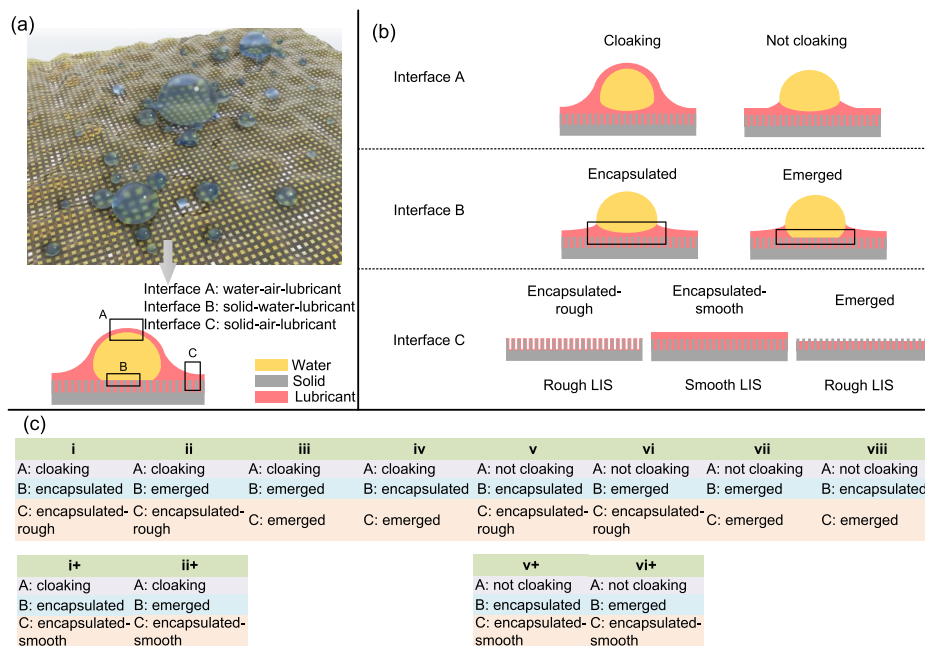


Figure 2. Description of interfaces in a lubricant-impregnated system. (a) Schematic diagram of LIS. There are three interfaces in this four-component system: interface A (water–air–oil), interface B (solid–water–oil), and interface C (solid–air–oil); (b) there are four factors influencing surface states (interface A, interface B, interface C and lubricant thickness), and each possible state is shown. The encapsulated-rough and emerged state of interface C are described as rough LIS and smooth LIS to describe the encapsulated-smooth state, respectively. (c) Twelve cases of all the possible states combinations on LIS. Every case is labeled for the convenience of analysis. The first row refers to rough LIS cases, and the second row refers to smooth LIS.

Table 2. Energy Parameter Settings

parameter [eV]		cloaking	not cloaking
interface A	ϵ_{CT-W}	0.0186	0.0152
interface B			
parameter [eV]		encapsulated	emerged
encapsulated	ϵ_{CT-Pt}	0.02	0.02
	ϵ_{W-Pt}	0.013	0.033
emerged	ϵ_{CT-Pt}	0.01	0.01
	ϵ_{W-Pt}	0.005	0.02

solid, and air, respectively. ψ is the shape factor with $\psi = (2 + \cos \theta)(1 - \cos \theta)^2$, and the contact angle of water on solid in the corresponding air $\theta_{ws(a)}$ is for calculating ψ_1 , as shown in panel I in Figure 3a.

In State II, nucleation occurs at the lubricant–solid interface, and the surface energy term is given by

$$E_{II} = \gamma_{ws}A_{ws} + \gamma_{wo}A_{wo} - \gamma_{so}A_{so} = \psi_2\pi\left(\frac{3V}{\pi\psi_2}\right)^{2/3}\gamma_{wo} \quad (2)$$

where the subscript o refers to the lubricant. The contact angle of water on solid in the lubricant $\theta_{ws(o)}$ is for calculating ψ_2 , as shown in panel II in Figure 3a.

Different from the discussion in ref 36, the surface energy of State III is divided into two situations for discussion in present work: cloaking state and not-cloaking state. The nuclei will form a lens if the condensate itself does not wet the lubricant and the lubricant does not cloak the condensate. The surface energy term in this circumstance is given by

$$E_{III}^{\text{not cloaking}} = \gamma_{wo}A_{wo} + \gamma_{wa}A_{wa} - \gamma_{oa}A_{oa} = \pi\left(\frac{3V}{\pi\lambda}\right)^{2/3}\xi\frac{\sin\theta_{wa}}{\sin\theta_{wo}}\gamma_{wa} \quad (3)$$

$$\text{with } \lambda = \frac{\sin\theta_{wo}(2 + \cos\theta_{wo})}{(1 + \cos\theta_{wo})^2} + \frac{\sin\theta_{wa}(2 + \cos\theta_{wa})}{(1 + \cos\theta_{wa})^2}, \quad \text{and} \\ \xi = \left(\frac{2}{1 + \cos\theta_{wo}} - \cos\theta_{wo}\right) + \frac{\sin\theta_{wo}}{\sin\theta_{wa}}\left(\frac{2}{1 + \cos\theta_{wa}} - \cos\theta_{wa}\right).$$

Here, θ_{wa} and θ_{wo} are two lens angles with respect to the plane of the lubricant, schematic in panel III in Figure 3a. To obtain these two lens angles, a simple two-dimensional simulation is conducted. Hexane beads (14 400) are first constructed to get enough thickness. Then, a nanodroplet of 3792 water beads is placed above hexane with prudent distance. The computational box size is $540 \times 570 \times 22 \text{ \AA}^3$, and the periodic boundary condition is applied to all of the three directions. This system is then equilibrated at 300 K using a Nose/Hoover thermostat with a timestep of 10 fs for 0.5 ns. After that, snapshots of system morphologies are collected for another 0.5 ns to get lens angles.

For the case that the lubricant can cloak condensates, droplets nucleate at the air–lubricant interface and will be cloaked by the lubricant subsequently. The cloaking leads to submergence of droplets in the lubricant due to capillary force, creating a fresh air–lubricant interface. Therefore, the surface energy term in this condition is given by

$$E_{III}^{\text{cloaking}} = \gamma_{wo}A_{wo} = 4\pi\left(\frac{3V}{4\pi}\right)^{2/3}\gamma_{wo} \quad (4)$$

Based on the surface energy terms above, the most preferable nucleation pathway can be identified. Comparing

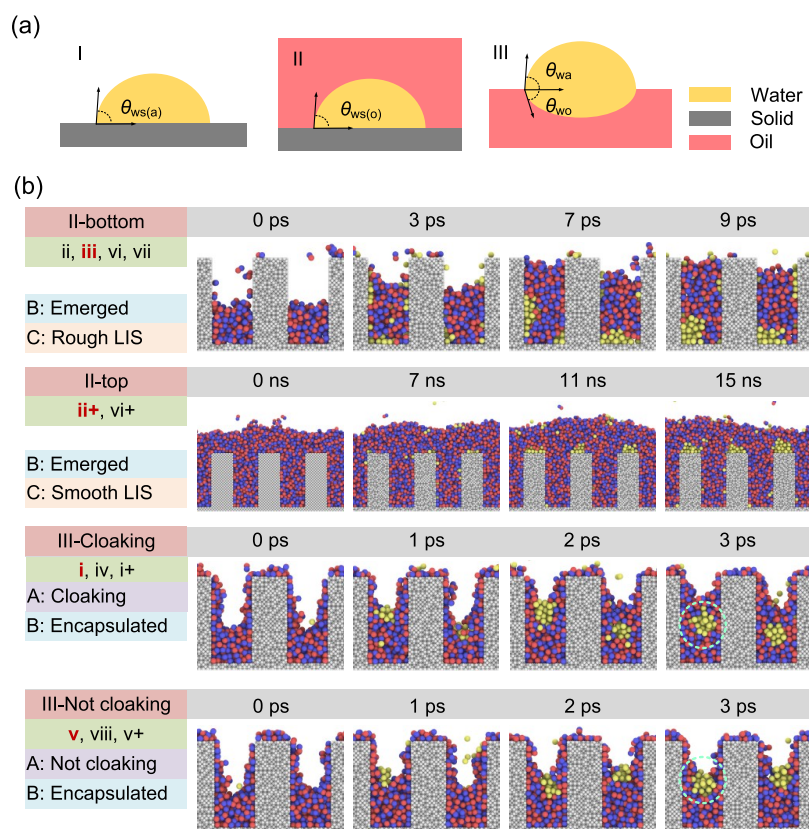
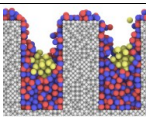
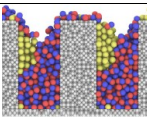
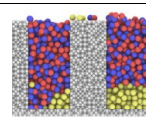
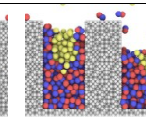


Figure 3. (a) Illustration of the possible nucleation sites of LIS: the air–solid interface (State I), the lubricant–solid interface (State II) and the air–lubricant interface (State III). The subscripts w, a, o, and s denote droplet, air, oil, and solid surface, respectively. (b) Four nucleation mechanisms are summarized from all of the 12 cases: II-bottom (nucleating at the solid–oil interface and the top of pillars), II-top (nucleating at the solid–oil interface and the bottom between pillars), III-cloaking (nucleating at the oil–air interface and then cloaked by the lubricant), and III-not cloaking (nucleating at the oil–air interface). The cases shown as examples are marked in red color. Interface states of each mechanism are also marked.

Table 3. Nucleation Site Calculation of LIS in the Cloaking States

Case	i, i+	ii, ii+	iii	iv
Interface A	Cloaking			
Interface B	Encapsulated	Emerged	Emerged	Encapsulated
Interface C	Encapsulated	Encapsulated	Emerged	Emerged
Snapshots of nucleation sites				
Computation	III	II	II	III
γ_{oa} [mN/m]	16.89	16.89	16.89	16.89
γ_{wo} [mN/m]	43.92	43.92	43.92	43.92
γ_{wa} [mN/m]	69	69	69	69
$\theta_{ws(a)}$ [°]	130	38	77.5	142
$\theta_{ws(o)}$ [°]	180	97	112	180
ψ_1	3.66	0.13	1.36	3.87
ψ_2	4	2.36	3.07	4
E_{II}/E_I	—	—	0.84	0.64
E_{III}/E_I	—	—	0.91	0.64
E_{III}/E_{II}	1	1.19	1.09	1
Theory	III	II	II	III

Table 4. Nucleation Site Calculation of LIS in the Not Cloaking States

Case	v, v+	vi, vi+	vii	viii
Interface A	Not cloaking			
Interface B	Encapsulated	Emerged	Emerged	Encapsulated
Interface C	Encapsulated	Encapsulated	Emerged	Emerged
Snapshots of nucleation sites				
Computation	III	II	II	III
γ_{oa} [mN/m]	16.31	16.31	16.31	16.31
γ_{wo} [mN/m]	62.58	62.58	62.58	62.58
γ_{wa} [mN/m]	72.06	72.06	72.06	72.06
$\theta_{ws(a)}$ [°]	120	35	80	154
$\theta_{ws(o)}$ [°]	180	97	90	180
θ_{wa} [°]	24	24	24	24
θ_{wo} [°]	120	120	120	120
$\sin\theta_{wa}$	0.41	0.41	0.41	0.41
$\sin\theta_{wo}$	0.87	0.87	0.87	0.87
$\cos\theta_{wa}$	0.91	0.91	0.91	0.91
$\cos\theta_{wo}$	-0.50	-0.50	-0.50	-0.50
ψ_1	3.37	0.09	1.48	3.97
ψ_2	4	2.36	2	4
λ	5.52	5.52	5.52	5.52
ξ	4.78	4.78	4.78	4.78
E_{II}/E_I	—	—	0.96	0.87
E_{III}/E_I	—	—	0.63	0.45
E_{III}/E_{II}	0.96	1.15	1.22	0.96
Theory	III	II	II	III

State I and State II, the nucleation on the lubricant–solid interface (State II) is preferable if satisfying

$$\frac{E_{II}}{E_I} = \left(\frac{\psi_2}{\psi_1} \right)^{1/3} \frac{\gamma_{wo}}{\gamma_{wa}} < 1 \quad (5)$$

Comparing State III and State I, the nucleation on the air–lubricant interface (State III) is preferable if satisfying

$$\frac{E_{III}^{\text{not cloaking}}}{E_I} = \frac{\xi}{(\psi_1 \lambda^2)^{1/3}} \frac{\sin \theta_{wa}}{\sin \theta_{wo}} < 1, \text{ or } \frac{E_{III}^{\text{cloaking}}}{E_I} = \left(\frac{4}{\psi_1} \right)^{1/3} \frac{\gamma_{wo}}{\gamma_{wa}} < 1 \quad (6)$$

Comparing State III and State II, the nucleation on the air–lubricant interface (State III) is preferable if satisfying

$$\frac{E_{III}^{\text{not cloaking}}}{E_{II}} = \frac{\xi}{(\psi_2 \lambda^2)^{1/3}} < 1, \text{ or } \frac{E_{III}^{\text{cloaking}}}{E_{II}} = \left(\frac{4}{\psi_2} \right)^{1/3} < 1 \quad (7)$$

Thus, we are able to determine which state is more preferable by calculating and comparing these three possible states. Calculation results are listed in Tables 3 and 4. Nucleation sites are determined by surface free energies. It can

also be concluded that the nucleation sites are only affected by interface B, independent of interface A, interface C, and lubricant thickness. Note that consistencies of nucleation sites between the theory and simulation results can also be a verification of the present computation method.

Nucleation Mechanisms. It is interesting to note that differences of nucleation behaviors are found in cases with the same nucleation sites. Nucleation processes of all of the 12 cases are summarized into four mechanisms as shown in Figure 3b. Snapshots of cases iii, ii+, i, and v are presented as examples.

For the cases with nucleation sites in state II, two mechanisms are found. Nucleation occurs at the bottom between pillars in cases ii, iii, vi, and vii, which are marked as II-bottom. In contrast, nucleation is observed on the top of pillars in cases ii+ and vi+, which are marked as II-top. For case iii, interface C is in the emerged state and nanopillars are exposed as a result. Also, water prefers to nucleate and grow at the lubricant–vapor interface compared to the solid–vapor interface. Thus, the lubricant–solid interface is directly available for water to nucleate and water clusters are found at the side and bottom surfaces of pillars at 3 ps, see Figure 3b. Nucleation continues and clusters are finally found at the bottom between pillars at 9 ps. As for II-top case, interface C is in the encapsulated-smooth state, which means that the nucleation sites, that is, the lubricant–solid interface, are all

wrapped by the lubricant. The top, side, and bottom of pillar surfaces are all potential nucleation sites. After diffusing through the lubricant, water particles encounter the top of pillars first. Clusters are found at pillar tops as a result. It should also be noted that due to the inevitable diffusion through the lubricant, the nucleation process is very slow. The cluster is observed as late as 15 ns. In summary, these two nucleation mechanisms are caused by different interface C states. When interface C is rough LIS, the nucleation mechanism is II-bottom. When interface C is smooth LIS, the nucleation mechanism is II-top.

For the cases with nucleation sites in state III, two mechanisms are also found. Nucleation sites are the air–lubricant interface (State III) if interface B is in the encapsulated interface. Particularly, if interface A is in the cloaking state, water will first nucleate at the air–lubricant interface and then is cloaked by the lubricant, which is named as III-cloaking. If interface A is not in the cloaking state, water will always nucleate and grow larger at the air–lubricant interface, which is named as III-not cloaking. The different cluster states are marked by the dashed circles in Figure 3b. Overall, nucleation sites are only affected by interface B state, but states of interfaces A and C should also be taken into consideration when studying the nucleation mechanisms.

Droplet Growth and Coalescence on LIS. After nucleation, droplets start to grow and merge with each other. The droplet dynamic behaviors of all of the 12 cases are investigated, see Figure S1 and S2 in the Supporting Information. It is found that the nucleation mechanisms directly influence the following droplet growth process, leading to different growth behaviors. Moreover, although having no effect on the nucleation mechanisms of III-cloaking and III-not cloaking, the lubricant thickness can result in different growing behaviors. Thus, six growth modes are summarized as shown in Figure 4a. Snapshots of case iii, ii+, i, i+, v, and v+ during condensation along with time are given as examples. For comparison, condensation on the superhydrophobic surface is also presented.

It is observed first that for the superhydrophobic surface, the droplet has a large contact angle (around 150°) and keeps good superhydrophobicity for static wettability. However, water nucleates and floods on the condensed surface during condensation. Different from the flooding mode found on the superhydrophobic surface, droplets generate for most cases on LIS and only flood in case iii. In case iii, water nucleates at the lubricant–solid interface and grows. Lubricants are therefore driven out of pillar intervals with water growing, which is defined as displacement in the present paper. However, displacement is not observed in case ii+, even though the nucleation site of which is as the same (lubricant–solid interface) as case iii, which is mainly attributed to the nucleation mechanism difference. Droplets nucleate at pillar tops in case ii+ (II-top). The growing and merging behaviors both happen at pillar tops and the lubricants at pillar intervals will not be affected. After growing and merging, droplets get larger and are lifted by the lubricant as well as the solid pillars. The lubricant is found favorable for droplet formation.

For the cases i and v, interface C is rough and fully wrapped with lubricants due to the thin lubricant and the encapsulated state. Water is found to nucleate and grow at gap intervals at first. After growing large enough, droplets at intervals begin to crop up through the lubricants and merge. Larger droplets are formed and lifted by the lubricant, staying in the slippery

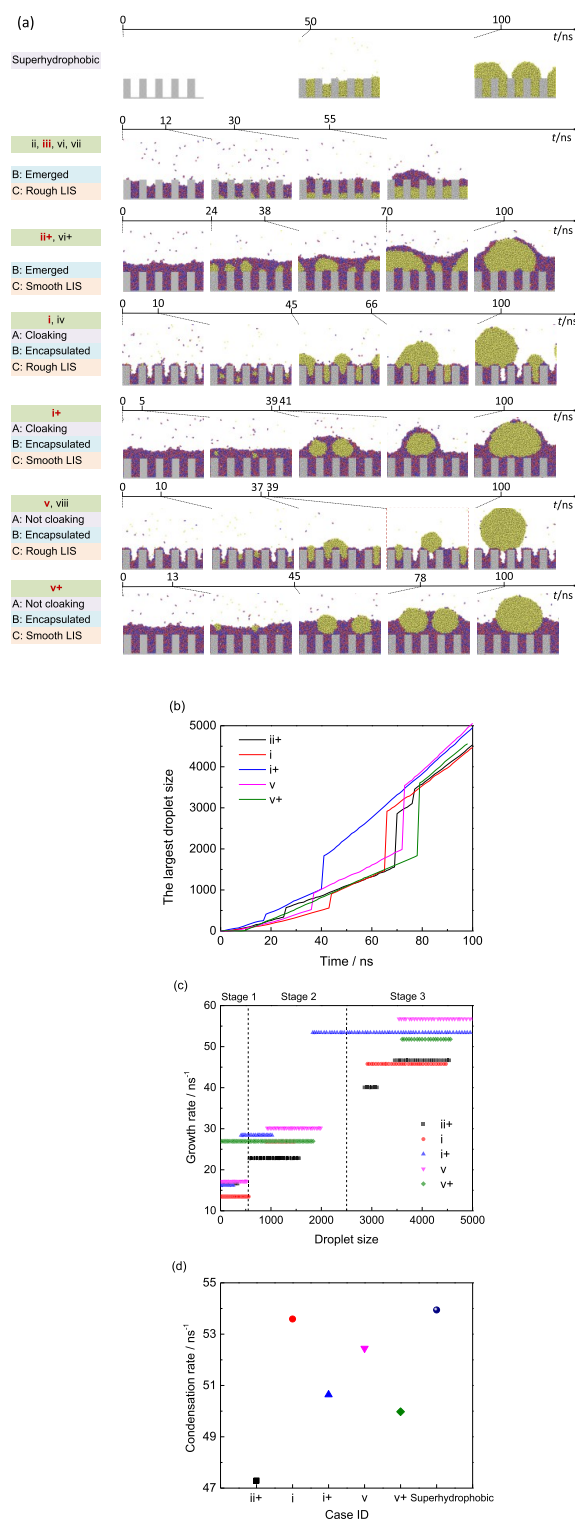


Figure 4. Droplet growth and coalescence behaviors on LIS. (a) Six growth modes are summarized and snapshots during condensation are shown along with time. The superhydrophobic case is also shown for comparison. (b) Largest droplet size along with time. (c) Growth rate along with the droplet size. Three growing stages are marked. (d) Averaged condensation rate of each case. The superhydrophobic case is given for comparison.

Wenzel state at the early stages.⁴⁵ Then, air pockets are formed, and the wetting transition is found, making droplets in slippery Cassie state. Note that case v has a much earlier

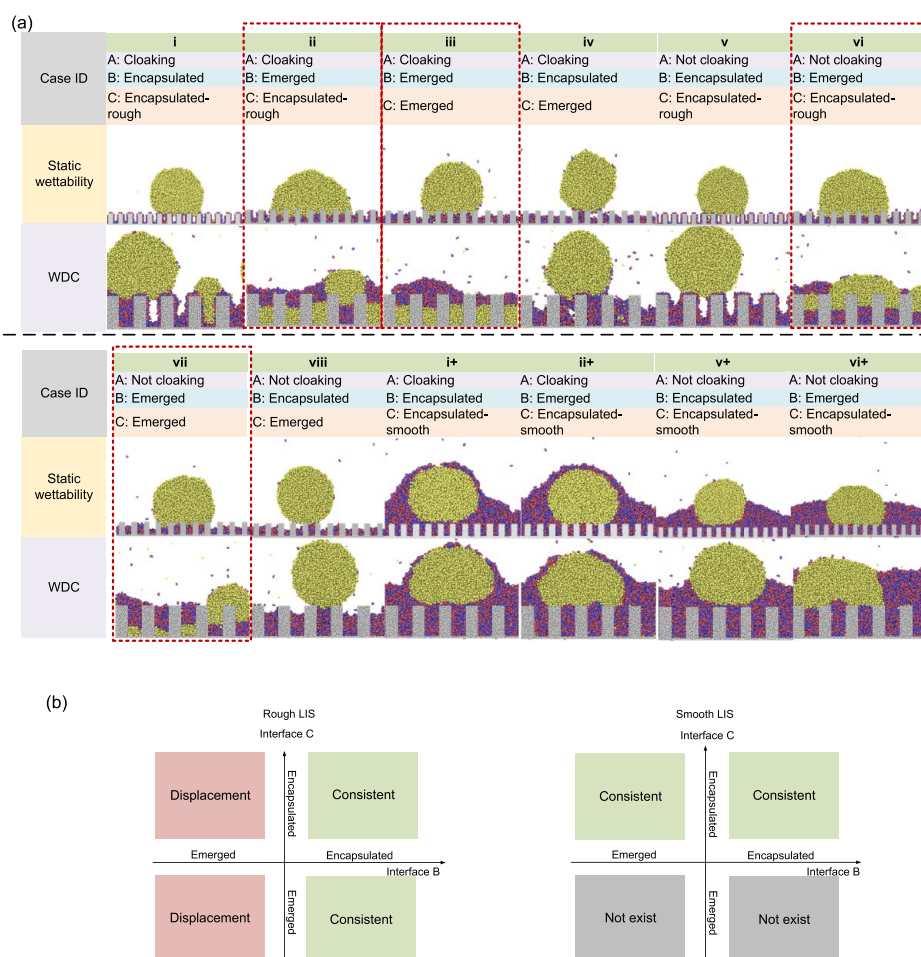


Figure 5. (a) WDC and the static wettability of water on LIS for all of the 12 cases. (b) Map for consistency between the WDC and static wettability. There are three states on the map: consistent (the WDC is consistent with the static wettability), displacement (the lubricant is driven out by the nucleated water), and not exist (the state does not exist under these interface states). The map is sorted into two conditions: rough LIS and smooth LIS. The abscissa represents the state of interface B (emerged or encapsulated) and the ordinate represents the state of interface C (emerged or encapsulated).

wetting transition (at 39 ns) than case i (at 100 ns), which might be attributed to the larger interface tension difference between water and lubricant of case v. Also, even though the interface A is in the cloaking state in case i, the cloaking state is not found after droplets grow larger to crop up through the lubricants from the interval. It is because the lubricant is too thin to wrap the droplet on rough LIS and can only cover the small interval droplets temporarily. For cases i+ and v+, the corresponding thicker lubricant conditions of cases i and v, droplets are found afloat on the lubricant all the time during their growing and coalescence process. The rough structures exist only for holding lubricant instead of affecting the WDC behavior. No wetting transition is found on smooth LIS due to the thick lubricant.

The droplet growth and coalescence characters are also quantitatively studied and shown in Figure 4b–d. Case iii is not considered because lubricants will be driven out of pillar intervals as water condenses. Figure 4b gives the largest droplet size along with time on these five surfaces. Droplets are getting larger by nucleating and merging. It is also found that the droplet growth rate gets larger with the droplet growing and keeps constant during a certain range of the droplet size. Thus, the curve slopes of Figure 4b are calculated and plotted along with the droplet size in Figure 4c. It is found that the droplet

growth can be classified into three stages based on the droplet size: 0–550 (stage 1), 550–2500 (stage 2), and 2500–5000 (stage 3). The droplet in case v grows faster and becomes the fastest in stages 2 and 3. It is interesting to note that the corresponding smooth case of case v, that is, case v+, grows the fastest in the beginning, but gets slower when the droplet merge occurs in case v but only one time in case v+. The rough oil–vapor interface and more times of droplets merging contribute to the fastest droplet growth of case v.

We also analyze the overall water growth rate and average it with time for each case, which is represented as the condensation rate in Figure 4d. The rough LIS cases, i and v, have larger condensation rate than the smooth LIS cases, i+ and v+, which might be attributed to the area of nucleation sites. Water will nucleate at the air–lubricant interface for all these four cases, but the area for nucleation is larger on rough LIS, resulting in a larger condensation rate. The lubricant will impede the condensation process compared to the superhydrophobic surface. Still, case i has a comparable value with the superhydrophobic case. Moreover, in contrast to the flooding mode on the superhydrophobic case, dropwise condensation is observed on case i.

The present simulation can help to reveal nucleation mechanisms and explain the phenomena observed in experiments. For example, Kajiya et al.³⁶ conducted an experimental study of condensation on the lubricant-impregnated surface. Regular alignment of water droplets was observed, which was afloat on the lubricant surface at the initial stage of condensation. Because of the limitations of the experiment, the nucleation process cannot be directly observed. However, the droplet formation can be explained by the present simulation results. The droplets were able to keep afloat in the experiment, and the water–air–oil was in not-cloaking condition. Therefore, droplets should be in the state of case v or v+ in the present study. Thus, corresponding nucleation processes can be looked up in Figure 4a that explains the float droplets in experiments.

Consistency Between the WDC and Static Wettability. After nucleation, growth, and coalescence, a comparatively large droplet is able to form on the lubricant-impregnated surface. We are able to compare the WDC and the static wettability of water on LIS. All of the 12 types of possible interface state combinations are shown in Figure 5a. The case labels as well as the corresponding interface states are also shown. Discrepancies between the WDC and the static wettability are found in cases ii, iii, vi, and vii, which are marked by the dashed boxes. Droplets can form and are lifted by the lubricant for their static wettability, but lubricants are driven out of pillar intervals and the displacement phenomenon occurs after condensation. Consistencies between the WDC and the static wettability are found for the other cases.

Note that the consistency between the WDC and the static wettability is related to the lubricant thickness. Displacements are found for cases ii and vi on rough LIS, while consistencies remain for cases ii+ and vi+ on smooth LIS. For smooth LIS, although water nucleates at the lubricant–solid interface, displacement is not observed, see case vi+ in Figure 3. This is a benefit from the thick lubricant. Because of the increased lubricant thickness, the nucleation mechanism is changed from II-bottom to II-top. Most droplets grow and merge at the top of nanostructures and the displacement therefore does not happen. Lubricant cover is favorable for the consistency between the WDC and static wettability in these circumstances.

To find out principles lying in the wettability discrepancy, the simulation results are summarized with a judging map, see Figure 5b. The map is divided into two types: rough LIS and smooth LIS. The abscissa represents the state of interface B (emerged or encapsulated), while the ordinate represents the state of interface C (emerged or encapsulated). It is easy to conclude from the map that the displacement will only occur on rough LIS if interface B is in the emerged state. Water will nucleate at the lubricant–solid interface, and displacement happens as droplets grow, see case iii in Figures 3 and 4. Other findings can also be found which might be useful for future LIS applications. The consistency of the WDC and the static wettability is nothing to do with the interface A. The consistency will always keep on smooth LIS if it exists. If interface B is in the encapsulated state, that is, the droplet could be lifted by the lubricant, there will always be consistency if it exists. The displacement will not happen if nucleation appears at the lubricant–vapor interface, and the WDC is as the same as the static wetting. This judging map is expected to provide instructions for determining whether consistency keeps for water on LIS under a certain condition.

CONCLUSIONS

We have studied the dynamic WDC of LIS by constructing a condensation system using the molecular dynamics method. Water nucleation, growth, and coalescence behaviors on LIS were presented and systematically discussed. It is found that nucleation occurs either on the air–lubricant interface or the lubricant–solid interface depending on the solid–water–oil interface state. Moreover, the nucleation process can be classified into four nucleation mechanisms: II-bottom, II-top, III-cloaking, and III-not cloaking. As condensation continues, six growing modes are identified. Wetting transitions from the slippery Wenzel state to the slippery Cassie state are found when the solid–water–oil interface is in the encapsulated-rough state. The lubricant can impede the condensation process compared to the superhydrophobic surface, but it is favorable for droplet formation and wetting transition. Discrepancies between the WDC and the static wettability have been found on rough LIS if the solid–water–oil interface is in the merged state. Lubricants will be driven out of pillar intervals and the displacement phenomenon occurs, which is caused by the nucleation at oil–solid interface. Finally, a map is proposed to conveniently decide whether displacement appears on LIS. Findings from this work substantially enrich our understanding of the WDC on LIS and its differences from corresponding static wettability. It is also expected to provide advices for the surface design in various applications, especially involved with the phase change.

ASSOCIATED CONTENT

Supporting Information

The Supporting Information is available free of charge at <https://pubs.acs.org/doi/10.1021/acsami.0c03018>.

Droplet static wettability and dynamic wettability during condensation on rough LIS and smooth LIS (PDF)

AUTHOR INFORMATION

Corresponding Authors

G. H. Tang – MOE Key Laboratory of Thermo-Fluid Science and Engineering, School of Energy and Power Engineering, Xi'an Jiaotong University, Xi'an 710049, P. R. China; orcid.org/0000-0002-7881-2573; Email: ghtang@mail.xjtu.edu.cn

Satish Kumar – G. W. Woodruff School of Mechanical Engineering, Georgia Institute of Technology, Atlanta, Georgia 30332, United States; Email: satish.kumar@me.gatech.edu

Author

Lin Guo – MOE Key Laboratory of Thermo-Fluid Science and Engineering, School of Energy and Power Engineering, Xi'an Jiaotong University, Xi'an 710049, P. R. China

Complete contact information is available at: <https://pubs.acs.org/doi/10.1021/acsami.0c03018>

Author Contributions

The manuscript was written through the contributions of all the authors. All the authors have given approval to the final version of the manuscript.

Notes

The authors declare no competing financial interest.

ACKNOWLEDGMENTS

We gratefully acknowledge the financial supports from the National Natural Science Foundation of China under Grant nos. 51825604 and 51721004, and the 111 Project under grant no. B16038.

REFERENCES

- (1) Dorrer, C.; R uhe, J. Some Thoughts on Superhydrophobic Wetting. *Soft Matter* **2009**, *5*, 51–61.
- (2) Young, T., III An Essay on the Cohesion of Fluids. *Philos. Trans. R. Soc. London* **1805**, *95*, 65–87.
- (3) Kwok, D. Y.; Neumann, A. W. Contact Angle Measurement and Contact Angle Interpretation. *Advances in Colloid and Interface Science* **1999**, *81*, 167–249.
- (4) Park, J.; Pasaogullari, U.; Bonville, L. Wettability Measurements of Irregular Shapes with Wilhelmy Plate Method. *Applied Surface Science* **2018**, *427*, 273–280.
- (5) Feng, J.; Pang, Y.; Qin, Z.; Ma, R.; Yao, S. Why Condensate Drops Can Spontaneously Move Away on Some Superhydrophobic Surfaces but Not on Others. *ACS Appl. Mater. Interfaces* **2012**, *4*, 6618–6625.
- (6) Wong, T.-S.; Kang, S. H.; Tang, S. K. Y.; Smythe, E. J.; Hatton, B. D.; Grinthal, A.; Aizenberg, J. Bioinspired Self-Repairing Slippery Surfaces with Pressure-Stable Omniphobicity. *Nature* **2011**, *477*, 443–447.
- (7) Lafuma, A.; Qu er e, D. Slippery Pre-Suffused Surfaces. *Epl* **2011**, *96*, 56001.
- (8) Smith, J. D.; Dhiman, R.; Anand, S.; Reza-Garduno, E.; Cohen, R. E.; McKinley, G. H.; Varanasi, K. K. Droplet Mobility on Lubricant-Impregnated Surfaces. *Soft Matter* **2013**, *9*, 1772–1780.
- (9) Hao, C.; Li, J.; Liu, Y.; Zhou, X.; Liu, Y.; Liu, R.; Che, L.; Zhou, W.; Sun, D.; Li, L.; Xu, L.; Wang, Z. Superhydrophobic-Like Tunable Droplet Bouncing on Slippery Liquid Interfaces. *Nat. Commun.* **2015**, *6*, 7986.
- (10) Chen, H.; Zhang, L.; Zhang, Y.; Zhang, P.; Zhang, D.; Jiang, L. Uni-Directional Liquid Spreading Control on a Bio-Inspired Surface from the Peristome of *Nepenthes alata*. *J. Mater. Chem. A* **2017**, *5*, 6914–6920.
- (11) Irajizad, P.; Ray, S.; Farokhnia, N.; Hasnain, M.; Baldelli, S.; Ghasemi, H. Remote Droplet Manipulation on Self-Healing Thermally Activated Magnetic Slippery Surfaces. *Adv. Mater. Interfaces* **2017**, *4*, 1700009.
- (12) Cao, J.; An, Q.; Liu, Z.; Jin, M.; Yan, Z.; Lin, W.; Chen, L.; Li, P.; Wang, X.; Zhou, G.; Shui, L. Electrowetting on Liquid-Infused Membrane for Flexible and Reliable Digital Droplet Manipulation and Application. *Sens. Actuators, B* **2019**, *291*, 470–477.
- (13) Jiang, J.; Gao, J.; Zhang, H.; He, W.; Zhang, J.; Daniel, D.; Yao, X. Directional Pumping of Water and Oil Microdroplets on Slippery Surface. *Proc. Natl. Acad. Sci. U.S.A.* **2019**, *116*, 2482–2487.
- (14) Wang, Z.; Xu, Q.; Wang, L.; Heng, L.; Jiang, L. Temperature-Induced Switchable Interfacial Interactions on Slippery Surfaces for Controllable Liquid Manipulation. *J. Mater. Chem. A* **2019**, *7*, 18510–18518.
- (15) Zhang, Y.; Jiao, Y.; Chen, C.; Zhu, S.; Li, C.; Li, J.; Hu, Y.; Wu, D.; Chu, J. Reversible Tuning between Isotropic and Anisotropic Sliding by One-Direction Mechanical Stretching on Microgrooved Slippery Surfaces. *Langmuir* **2019**, *35*, 10625–10630.
- (16) Wang, P.; Zhang, D.; Sun, S.; Li, T.; Sun, Y. Fabrication of Slippery Lubricant-Infused Porous Surface with High Underwater Transparency for the Control of Marine Biofouling. *ACS Appl. Mater. Interfaces* **2017**, *9*, 972–982.
- (17) Doll, K.; Yang, I.; Fadeeva, E.; Kommerein, N.; Szafranski, S. P.; Bei der Wieden, G.; Greuling, A.; Winkel, A.; Chichkov, B. N.; Stumpp, N. S.; Stiesch, M. Liquid-Infused Structured Titanium Surfaces: Antiadhesive Mechanism to Repel *Streptococcus oralis* Biofilms. *ACS Appl. Mater. Interfaces* **2019**, *11*, 23026–23038.
- (18) Wang, J.; Huang, Y.; You, K.; Yang, X.; Song, Y.; Zhu, H.; Xia, F.; Jiang, L. Temperature-Driven Precise Control of Biological Droplet's Adhesion on a Slippery Surface. *ACS Appl. Mater. Interfaces* **2019**, *11*, 7591–7599.
- (19) Yang, C.; He, G.; Zhang, A.; Wu, Q.; Zhou, L.; Hang, T.; Liu, D.; Xiao, S.; Chen, H.-J.; Liu, F.; Li, L.; Wang, J.; Xie, X. Injectable Slippery Lubricant-Coated Spiky Microparticles with Persistent and Exceptional Biofouling-Resistance. *ACS Cent. Sci.* **2019**, *5*, 250–258.
- (20) Wang, Y.; Qian, B.; Lai, C.; Wang, X.; Ma, K.; Guo, Y.; Zhu, X.; Fei, B.; Xin, J. H. Flexible Slippery Surface to Manipulate Droplet Coalescence and Sliding, and Its Practicability in Wind-Resistant Water Collection. *ACS Appl. Mater. Interfaces* **2017**, *9*, 24428–24432.
- (21) Agrawal, P.; Salomons, T. T.; Chiriac, D. S.; Ross, A. C.; Oleschuk, R. D. Facile Actuation of Organic and Aqueous Droplets on Slippery Liquid-Infused Porous Surfaces for the Application of On-Chip Polymer Synthesis and Liquid-Liquid Extraction. *ACS Appl. Mater. Interfaces* **2019**, *11*, 28327–28335.
- (22) Xu, W.; Zhou, X.; Hao, C.; Zheng, H.; Liu, Y.; Yan, X.; Yang, Z.; Leung, M.; Zeng, X. C.; Xu, R. X.; Wang, Z. SLIPS-TENG: Robust Triboelectric Nanogenerator with Optical and Charge Transparency using a Slippery Interface. *Natl. Sci. Rev.* **2019**, *6*, 540–550.
- (23) Zhang, D.; You, H.; Yuan, L.; Hao, R.; Li, T.; Fang, J. Hydrophobic Slippery Surface-Based Surface-Enhanced Raman Spectroscopy Platform for Ultrasensitive Detection in Food Safety Applications. *Anal. Chem.* **2019**, *91*, 4687–4695.
- (24) Zhang, M.; Liu, Q.; Liu, J.; Yu, J.; Wang, J. Self-Healing Liquid-Infused Surfaces with High Transparency for Optical Devices. *Mrc* **2019**, *9*, 92–98.
- (25) Goudie, M. J.; Pant, J.; Handa, H. Liquid-Infused Nitric Oxide-Releasing (LINORel) Silicone for Decreased Fouling, Thrombosis, and Infection of Medical Devices. *Sci. Rep.* **2017**, *7*, 13623.
- (26) Guo, L.; Tang, G. H.; Kumar, S. Droplet Morphology and Mobility on Lubricant-Impregnated Surfaces: A Molecular Dynamics Study. *Langmuir* **2019**, *35*, 16377–16387.
- (27) Park, K.-C.; Kim, P.; Grinthal, A.; He, N.; Fox, D.; Weaver, J. C.; Aizenberg, J. Condensation on Slippery Asymmetric Bumps. *Nature* **2016**, *531*, 78–82.
- (28) Guo, L.; Tang, G. H. Dropwise Condensation on Bioinspired Hydrophilic-Slippery Surface. *RSC Adv.* **2018**, *8*, 39341–39351.
- (29) Sun, J.; Weisensee, P. B. Microdroplet Self-Propulsion During Dropwise Condensation on Lubricant-Infused Surfaces. *Soft Matter* **2019**, *15*, 4808–4817.
- (30) Sirohia, G. K.; Dai, X. Designing Air-Independent Slippery Rough Surfaces for Condensation. *Int. J. Heat Mass Transfer* **2019**, *140*, 777–785.
- (31) Wang, R.; Hong, S.; Huang, X.; Liu, H. Stable Magnetic Fluid Anti-Icing Surfaces Supported by a Magnetic Field and Porous Substrate. *Mater. Res. Express* **2019**, *6*, 055035.
- (32) Zhang, M.; Chen, R.; Liu, Q.; Liu, J.; Yu, J.; Song, D.; Liu, P.; Gao, L.; Wang, J. Long-Term Stability of a Liquid-Infused Coating with Anti-Corrosion and Anti-Icing Potentials on Al Alloy. *ChemElectroChem* **2019**, *6*, 1–10.
- (33) Yamazaki, T.; Tenjimbayashi, M.; Manabe, K.; Moriya, T.; Nakamura, H.; Nakamura, T.; Matsubayashi, T.; Tsuge, Y.; Shiratori, S. Antifreeze Liquid-Infused Surface with High Transparency, Low Ice Adhesion Strength, and Antifrosting Properties Fabricated through a Spray Layer-by-Layer Method. *Ind. Eng. Chem. Res.* **2019**, *58*, 2225–2234.
- (34) Anand, S.; Paxson, A. T.; Dhiman, R.; Smith, J. D.; Varanasi, K. K. Enhanced Condensation on Lubricant-Impregnated Nanotextured Surfaces. *ACS Nano* **2012**, *6*, 10122–10129.
- (35) Xiao, R.; Miljkovic, N.; Enright, R.; Wang, E. N. Immersion Condensation on Oil-Infused Heterogeneous Surfaces for Enhanced Heat Transfer. *Sci. Rep.* **2013**, *3*, 1988.
- (36) Kajiyama, T.; Schellenberger, F.; Papadopoulos, P.; Vollmer, D.; Butt, H. J. 3D Imaging of Water-Drop Condensation on Hydrophobic and Hydrophilic Lubricant-Impregnated Surfaces. *Sci. Rep.* **2016**, *6*, 23687.
- (37) Anand, S.; Rykaczewski, K.; Subramanyam, S. B.; Beysens, D.; Varanasi, K. K. How Droplets Nucleate and Grow on Liquids and Liquid Impregnated Surfaces. *Soft Matter* **2015**, *11*, 69–80.

(38) Arenas, I.; García, E.; Fu, M. K.; Orlandi, P.; Hultmark, M.; Leonardi, S. Comparison between Superhydrophobic, Liquid Infused and Rough Surfaces: a Direct Numerical Simulation Study. *J. Fluid Mech.* **2019**, *869*, 500–525.

(39) Metya, A. K.; Singh, J. K. Ice Adhesion Mechanism on Lubricant-Impregnated Surfaces Using Molecular Dynamics Simulations. *Mol. Simul.* **2019**, *45*, 394–402.

(40) Xu, W.; Lan, Z.; Peng, B. L.; Wen, R. F.; Ma, X. H. Effect of Surface Free Energies on the Heterogeneous Nucleation of Water Droplet: a Molecular Dynamics Simulation Approach. *J. Chem. Phys.* **2015**, *142*, 054701.

(41) Gao, S.; Liao, Q.; Liu, W.; Liu, Z. Effects of Solid Fraction on Droplet Wetting and Vapor Condensation: A Molecular Dynamic Simulation Study. *Langmuir* **2017**, *33*, 12379–12388.

(42) Niu, D.; Tang, G. Molecular Dynamics Simulation of Droplet Nucleation and Growth on a Rough Surface: Revealing the Microscopic Mechanism of the Flooding Mode. *RSC Adv.* **2018**, *8*, 24517–24524.

(43) Chiu, S.-W.; Scott, H. L.; Jakobsson, E. A Coarse-Grained Model based on Morse Potential for Water and n-Alkanes. *J. Chem. Theory Comput.* **2010**, *6*, 851–863.

(44) Shinoda, W.; DeVane, R.; Klein, M. L. Multi-Property Fitting and Parameterization of a Coarse Grained Model for Aqueous Surfactants. *Mol. Simul.* **2007**, *33*, 27–36.

(45) Dai, X.; Stogin, B. B.; Yang, S.; Wong, T.-S. Slippery Wenzel State. *ACS Nano* **2015**, *9*, 9260–9267.